# Voltage and Frequency Stability of Weak Power Distribution Networks with Droop-Controlled Rotational and Electronic Distributed Generators

Zhao Wang[1] and Michael Lemmon[1]

**Abstract**

Distributed generations (DG's), based on both synchronous generators (SG's) and fast inverters, are incorporated to improve power quality and reliability of power grids. These DG's, however, may cause voltage and frequency stability issues due to weakness in power distribution networks. Weakness not only means significant ratios between resistance and reactance components in impedances (*lossy*), but also large power flow compared with rated power level (stressful). Weak networks complicate voltage stability and frequency synchronization analysis, because of coupled network dynamics. Additionally, droop controlled rotational and electronic DG's have different dynamics, making a comprehensive stability analysis even more difficult. This paper derives sufficient conditions for voltage stability and frequency synchronization of a weak power distribution network coupled with droop-controlled DG's, which are based on both fast inverters and SG's. These conditions are inequality constraints on network parameters, load levels and generation control commands. Simulation tests show that asymptotic voltage stability and frequency synchronization are ensured in a weak network, in both a modified 37-node test feeder and a rural electrification network model. Moreover, these stability conditions also provide guidance in robustly integrating DG's into existing power distribution networks.

## I. INTRODUCTION

Distributed generators (DG's) are usually organized in microgrids and installed to improve power quality and reliability in power distribution networks, by supplying power locally during main grid contingency events [1]. Power quality, measured in voltage magnitude and network

[1]The authors are with the Department of Electrical Engineering, University of Notre Dame, Notre Dame, IN 46556, USA. zwang6 and lemmon at nd.edu

frequency, is the primary concern of power network operations, especially for weak networks. Networks that are lossy may not be weak. Typically, a *lossy* network has its ratio between resistance and reactance $R/X$ (equivalently $G/B$) greater than one. Weak networks, however, have a large amount of power flow compared with the rated power level, described in a short-circuit ratio (SCR) in [2]. Connections of DG's, based on both fast inverters and synchronous generators (SG's), introduce multidirectional power flows that cause power quality problems in weak networks. Due to network weakness, dynamics of voltage and frequency are coupled, making it difficult to simultaneously guarantee voltage stability and frequency synchronization.

Stability analysis of power networks is a long-treated topic, but existing stability analysis approaches are not sufficient to analyze weak networks' voltage control and frequency synchronization conditions. Initial research efforts apply Lyapunov-based methods in [3], [4], [5], [6] to transient frequency stability analysis. Although closed-form stability conditions are obtained, strong networks are assumed without voltage control dynamics, improper for analyzing weak networks. To treat weak networks, research works in [7], [8], [9] checked small-signal stability using eigenvalue calculation of linearized network models. Not only linearized analysis applies to small neighborhoods of linearization points, there have also been no closed-form stability conditions for *weak* distribution networks coupled with DG's. Some work [10] attempts to address this issue by viewing the network as a set of coupled nonlinear oscillators, assuming voltages are kept within bounds. In their recent work [11], decoupled dynamics are incorporated and no voltage stability conditions are provided. Another recent paper [12] discusses frequency stability for a inverter-based microgrid, which is a *lossy* network with an large short-circuit ratio (above $60$). As an exception, small-signal stability analysis in [2] shows that an increasing power flow stress leads to instability. A measure of power flow stress (i.e. SCR) is used in this paper to characterize truly *weak* networks.

The stability analysis problem is further complicated by a hybrid network model including both rotational and electronic DG's. As in [13], such a hybrid network is treated as a multirate Kuramoto model to analyze frequency synchronization, but conditions there are hard to check. An equivalence is pointed out, in [14], of the dynamics of a synchronous generator and a fast inverter with low pass filters. This equivalence allows stability of a network with both rotational and electronic DG's being treated as a traditional multi-machine network. Building upon those prior works, this paper derives a set of inequality constraints whose satisfaction assures asymptotic voltage stability and frequency synchronization. Sufficient conditions are on network weakness, voltage control authority, and load levels, so that network states converge to an isolated equilibrium point within regulatory limits of power quality.

The remainder of this paper is organized as follows. Section II reviews the power system background and notations used throughout this paper. Section III presents the weak network model, with droop-controlled rotational and electronic DG's. Section IV presents the main results of this paper, i.e. sufficient conditions that ensure voltage stability and frequency synchronization. Section V demonstrates simulation results showing that sufficient conditions ensure asymptotic stability of voltage and frequency, providing guidance in how DG's should integrate into existing networks. Section VI provides concluding remarks and identifies future directions in weak network stability analysis.

## II. Background and Notations

Power flow relationships among buses and general load models are reviewed in this section. Before introducing those models, three-phase balanced operation and per-unit (p.u.) normalization are clarified as basic assumptions. Stability analyses in this paper build upon a balanced three-phase network model, which makes the analysis also applicable to single-phase cases. In addition, p.u. normalization is applied to accommodate various nominal voltage levels in a network.

Admittance matrix $Y$ is defined as in power system analysis textbooks [15], whose $ij$-th component is expressed as

$$Y_{ij} = \begin{cases} -\frac{1}{Z_{ij}} & \text{if bus i and j are connect,} \\ 0 & \text{else,} \end{cases}$$
$$Y_{ii} = \sum_{j=1, j\neq i}^{n} -Y_{ij},$$

where $Z_{ij}$ is the impedance between bus $i$ and $j$ for all $i, j \in \{1, 2, \ldots, n\}$. The admittance matrix $Y$ is also expressed in real and imaginary parts as $Y_{n\times n} = G_{n\times n} + jB_{n\times n}$, where $G_{n\times n}$ is the conductance matrix and $B_{n\times n}$ is the susceptance matrix.

Weak networks and lossy networks are different, and their differences must be clarified. Lossy networks simply have $|G_{ij}/B_{ij}| \geq 1$ for any $i \neq j$ in the admittance matrix $Y_{n\times n}$, which is equivalent to $|R_{ij}/X_{ij}| \geq 1$. In contrast, lossless networks are assumed to be with negligible $G_{ij}$, then there is a pure imaginary admittance matrix $Y_{n\times n} = jB_{n\times n}$, which brings about simplicity in network analysis. Weak networks, nevertheless, should be characterized from the perspective of power flow stress, such as the short-circuit ratio (SCR) defined in [2]. SCR is the ratio between the short circuit power at a generator's point of common coupling and the maximum apparent power of this generator. As indicated in [2], a network with $SCR \leq 10$ is considered to be *weak*, while one with $SCR \geq 20$ is *strong*. Connected to any bus $i$, there is a

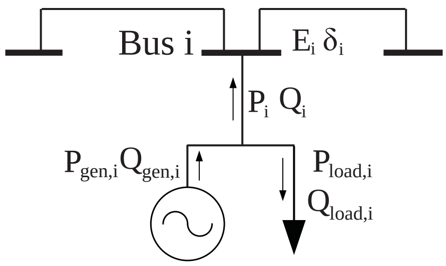


Fig. 1. Power Balance at Bus i

controlled generator and a synthesized load, as shown in Figure 1. At bus $i$ in Figure 1, $E_i$ is voltage magnitude and $\delta_i$ is phase angle; $P_i$ and $Q_i$ are the injected powers; $P_{gen,i}$ and $Q_{gen,i}$ are the total powers generated; $P_{load,i}$ and $Q_{load,i}$ denote the real and reactive loads. Powers injected into bus $i$ are

$$P_i = P_{gen,i} - P_{load,i}, \tag{1}$$

$$Q_i = Q_{gen,i} - Q_{load,i}. \tag{2}$$

Especially, pure load bus $j$ has $P_j + P_{load,j} = 0$ and $Q_j + Q_{load,j} = 0$.

Power balance relationships depict power exchanges between buses, derived from $S = P + jQ = VI^* = V(Y_{n\times n}V)^*$. In this equation: $P$ and $Q$ are $n$-dimensional real and reactive power vectors; $V$ and $I$ are complex voltage and current vectors. Real power injection $P_i$ and reactive power injection $Q_i$ at bus $i$ depend on states of neighboring buses, captured in the so called *power balance* relationships

$$P_i = \sum_{j=1}^{n} E_i E_j (G_{ij}\cos(\delta_i - \delta_j) + B_{ij}\sin(\delta_i - \delta_j)), \tag{3}$$

$$Q_i = \sum_{j=1}^{n} E_i E_j (G_{ij}\sin(\delta_i - \delta_j) - B_{ij}\cos(\delta_i - \delta_j)). \tag{4}$$

The real and reactive power vectors are closely coupled through sinusoidal functions in equations (3,4). With trivial $\{G_{ij}\}$ and phase shifts between buses, power balance relations are simplified as $P_i \approx \sum_{j=1}^{n} E_i E_j B_{ij}(\delta_i - \delta_j)$ and $Q_i \approx -\sum_{j=1}^{n} E_i E_j B_{ij}$. This simplified linear relations are the reason that many analysis efforts took this assumption, i.e. the strong network assumption. Nevertheless, for weak distribution networks coupled with DG's, system dynamics are coupled as in equations (3,4). This coupling nature in weak networks makes controlling DG's a challenging task. For example, injecting real power from DG's downstream a distribution feeder would not only change phase angles, but also increase voltage magnitudes at these DG's, which is the so-called "*voltage-rise problem*".

To incorporate various types of loads into $P_{load,i}$ and $Q_{load,i}$, a ZIP model is applied [16]. The ZIP model is a polynomial load model that combines constant impedance (Z), constant current (I) and constant power (P) components. The actual loads are defined as a function of voltage magnitudes $\{E_i\}$ in p.u., which is

$$P_{load,i} = E_i^2 P_{load,a,i} + E_i P_{load,b,i} + P_{load,c,i},$$
$$Q_{load,i} = E_i^2 Q_{load,a,i} + E_i Q_{load,b,i} + Q_{load,c,i},$$

where $P_{load,a,i}$ and $Q_{load,a,i}$ are nominal constant impedance loads, e.g. incandescent light bulbs and resistance heaters; $P_{load,b,i}$ and $Q_{load,b,i}$ are nominal constant current loads, usually representing active motor controllers; $P_{load,c,i}$ and $Q_{load,c,i}$ are nominal constant power loads, generally a result of active power control. Using second-order polynomials, this ZIP load model approximates a variety of load types.

## III. System Model

This section obtains system models of weak networks coupled with both rotational and electronic DG's. The equivalence is explained between dynamics of a rotational DG and a fast inverter with a low pass filter. Using the unified model, conditions are derived to establish an isolated equilibrium point. Phase angle dynamic equations of a network are then constructed in the form of nonlinear oscillators. With respect to the equilibrium point, voltage error dynamic equations are obtained. Definitions of both asymptotic frequency and voltage stability are then provided as objectives of stability analysis problems.

In this paper, inverter-based controllers are based on the CERTS (Consortium for Electric Reliability Technology Solutions) droop control mechanisms [1], which are modified versions of conventional droop controllers. For a total of $m$ inverter based DG's, the associated phase angle and voltage dynamic equations at the $i$th inverter based DG are

$$\dot{\delta}_i = m_P(P_{ref,i} - P_{gen,i}) + \omega_0 = m_P(P_{ref,i} - P_i - P_{load,i}) + \omega_0, \tag{5}$$

$$\dot{E}_i = K_Q(E_{ref,i} - E_i) - m_Q Q_{gen,i} = K_Q(E_{ref,i} - E_i) - m_Q(Q_i + Q_{load,i}), \tag{6}$$

for all $i \in \{1, 2, \ldots, m\}$, where $m_P$ is the droop slope of $P$-$f$ droop controller; $\omega_0$ is the nominal angular frequency; $K_Q$ and $m_Q$ are the voltage control gain and the droop slope of $Q$-$E$ droop controller, respectively. In equations above, $P_{ref,i}$ and $E_{ref,i}$ denote the commanded real power and voltage levels in the controller at the $i$th bus.

Dynamics of synchronous generators are typically described in swing equations. For the $i$th rotational DG, the dynamic equation of phase angles is

$$M_i\ddot{\delta}_i + D_i\dot{\delta}_i = P_{ref,i} - P_{gen,i} = P_{ref,i} - P_i - P_{load,i} \tag{7}$$

where $M_i$ is inertia of the machine and $D_i$ is damping of the rotator at bus $i$. It is assumed that voltages of these DG's are regulated by a similar mechanism used in equation (6).

As pointed out in [14], phase angle dynamics of a rotational DG are equivalent to a inverter-based DG with low pass filters. These low pass filters are included in DG controllers through real and reactive power measurements. Dynamics of these low-pass filters at the $i$th inverter-based DG are

$$\tau_{S,i}\dot{P}^m_{gen,i}(t) = -P^m_{gen,i}(t) + P_{gen,i}(t), \tag{8}$$

$$\tau_{S,i}\dot{Q}^m_{gen,i}(t) = -Q^m_{gen,i}(t) + Q_{gen,i}(t), \tag{9}$$

where $\tau_{S,i}$ is the time constant of power measurement at bus $i$; $P^m_i$ and $Q^m_i$ are measured powers used by inverter-based controllers.

These low-pass filters have different impacts on dynamics of phase angle and voltage. For phase angle dynamics, low-pass filters transform first-order equations to swing equations.

$$\begin{aligned}\frac{d}{dt}\dot{\delta}_i(t) &= -m_P \dot{P}^m_{gen,i}(t),\\ &= -\frac{m_P}{\tau_{S,i}}(-P^m_{gen,i}(t) + P_{gen,i}(t)),\\ &= \frac{m_P}{\tau_{S,i}}(P_{ref,i} - \frac{1}{m_P}\dot{\delta}_i(t) + \frac{1}{m_p}\omega_0 - P_{gen,i}(t)).\end{aligned}$$

The second-order dynamics of phase angle are rewritten as

$$\frac{\tau_{S,i}}{m_P}\ddot{\delta}_i(t) + \frac{1}{m_P}\dot{\delta}_i(t) = P_{ref,i} + \frac{1}{m_p}\omega_0 - P_{gen,i}(t),$$

which has exactly the same form as equation (7). With $m_P = \pi$ for CERTS droop controllers, the time constant $\tau_{S,i}$ cannot be neglected. For voltage dynamics, the impact of low-pass filters also leads to a second-order equation for the $i$th bus connected to an inverter-based DG.

$$\begin{aligned}\frac{d}{dt}\dot{E}_i(t) &= -K_Q\dot{E}_i(t)) - m_Q\dot{Q}^m_{gen,i}(t),\\ &= -K_Q\dot{E}_i(t)) - \frac{m_Q}{\tau_{S,i}}(-Q^m_{gen,i}(t) + Q_{gen,i}(t)),\\ &= -K_Q\dot{E}_i(t)) + \frac{K_Q}{\tau_{S,i}}(E_{ref,i} - E_i(t)) - \frac{1}{\tau_{S,i}}\dot{E}_i(t) - \frac{m_Q}{\tau_{S,i}}Q_{gen,i}(t),\end{aligned}$$

which is rewritten as

$$\tau_{S,i}\ddot{E}_i(t) + (K_Q\tau_{S,i} + 1)\dot{E}_i(t) + K_Q E_i(t) = K_Q E_{ref,i} - m_Q Q_i(t).$$

Time constants $\tau_{S,i}$'s are small compare with large $K_Q$, so that the dynamics can be simplified to the original first-order form as

$$\dot{E}_i(t) = K_Q(E_{ref,i} - E_i(t)) - m_Q Q_{gen,i}(t).$$

As a result, all analysis hereafter will be based on the second-order phase angle dynamics in equation (7) and first-order voltage dynamics in equation (6). To simplify our analysis, the following assumption is made about parameters in the second-order phase angle model.

*Assumption 1:* Dynamics of both inverter-based and rotating machine-based DGs are with the same parameters. This means that for a total of $m$ inverter-based DG coupled buses and $g$ SG-based DG coupled buses, there are $\frac{\tau_{S,1}}{m_P} = \ldots = \frac{\tau_{S,m}}{m_P} = M_1 = \ldots = M_g$ and $\frac{1}{m_P} = \ldots = \frac{1}{m_P} = D_1 = \ldots = D_g$.

To define equilibrium points of the complete system model in equations (3,4,6,7), a change of variable is necessary for phase angles. There is one surplus degree of freedom (DOF) in phase angles $\{\delta_i\}$. In a network with $n$ DG-coupled buses, to remove this additional DOF in $\{\delta_i\}$, phase angles of the first $(n-1)$ buses refer to a common bus, i.e. the $n$th bus. Define phase angle difference $\theta_i = \delta_i - \delta_n$ for all $i \in \{1, 2, \ldots, n-1\}$, hence $\theta_n = 0$. The equilibrium is expressed as $(P_{equ}, Q_{equ}, \theta_{equ}, E_{equ}, \omega_{equ})$, which is a zero point of the dynamic equations. Corresponding to a total number of $2n$ unknown states $(E_{equ}, \theta_{equ}, \omega_{equ})$, there are $2n$ equations $f(t) = [f_1; f_2; f_3]^T = 0$, where $f_1$, $f_2$, and $f_3$ are as follows

$$f_{1,i} = K_Q(E_{ref,i} - E_{equ,i}) - m_Q(Q_{equ,i}(E_{equ}, \theta_{equ}) + Q_{load,i}(E_{equ,i})), i \in \{1, 2, \ldots, n\} \tag{10}$$

$$\begin{aligned} f_{2,i} = & \frac{1}{M}(P_{ref,i} - P_{equ,i}(E_{equ}, \theta_{equ}) - P_{load,i}(E_{equ,i})) \\ & - \frac{1}{M}(P_{ref,n} - P_{equ,n}(E_{equ}, \theta_{equ}) - P_{load,n}(E_{equ,n})), i \in \{1, 2, \ldots, n-1\} \end{aligned} \tag{11}$$

$$f_3 = -\frac{D}{M}\omega_{equ} - \frac{1}{M}(P_{ref,n} + D\omega_0 - P_{equ,n}(E_{equ}, \theta_{equ}) - P_{load,n}(E_{equ,n})). \tag{12}$$

As long as the equilibrium point is an isolated solution to the nonlinear equations, asymptotic stability can be discussed with respect to it. By analyzing the Jacobian matrix of the nonlinear equations $f(t)$, the following lemma establishes the existence of an isolated equilibrium point:

*Lemma 1:* For any given real power $\{P_{ref,i}\}$ and voltage $\{E_{ref,i}\}$ commands, if Jacobian matrices $\frac{\partial f_1}{\partial E_{equ}}$, $\frac{\partial f_2}{\partial \theta_{equ}}$, as well as matrices $(I - (\frac{\partial f_1}{\partial E_{equ}})^{-1} \frac{\partial f_1}{\partial \theta_{equ}} (\frac{\partial f_2}{\partial \theta_{equ}})^{-1} \frac{\partial f_2}{\partial E_{equ}})$ and $(I - (\frac{\partial f_2}{\partial \theta_{equ}})^{-1} \frac{\partial f_2}{\partial E_{equ}} (\frac{\partial f_1}{\partial E_{equ}})^{-1} \frac{\partial f_1}{\partial \theta_{equ}})$ are full rank, then there is an isolated equilibrium point $(P_{equ}, Q_{equ}, \theta_{equ}, E_{equ}, \omega_{equ})$ for the complete system model in equations (3,4,10,11,12).

*Proof:* Jacobian of $f(t) = [f_1; f_2; f_3]^T$ in equations (10,11,12) is as follows:

$$J = \left( \begin{array}{c|cc} \frac{\partial f_1}{\partial E_{equ}} & \frac{\partial f_1}{\partial \theta_{equ}} & 0 \\ \hline \frac{\partial f_2}{\partial E_{equ}} & \frac{\partial f_2}{\partial \theta_{equ}} & 0 \\ \frac{\partial f_3}{\partial E_{equ}} & \frac{\partial f_3}{\partial \theta_{equ}} & -\frac{D}{M} \end{array} \right),$$

whose determinant is $det(\frac{\partial f_1}{\partial E_{equ}})\ det(\frac{\partial f_2}{\partial \theta_{equ}})\ det(I - (\frac{\partial f_2}{\partial \theta_{equ}})^{-1} \frac{\partial f_2}{\partial E_{equ}} (\frac{\partial f_1}{\partial E_{equ}})^{-1} \frac{\partial f_1}{\partial \theta_{equ}})$ or equivalently $det(\frac{\partial f_2}{\partial \theta_{equ}})\ det(\frac{\partial f_1}{\partial E_{equ}})\ det(I - (\frac{\partial f_1}{\partial E_{equ}})^{-1} \frac{\partial f_1}{\partial \theta_{equ}} (\frac{\partial f_2}{\partial \theta_{equ}})^{-1} \frac{\partial f_2}{\partial E_{equ}})$. The Jacobian maintains its rank, if and only if matrix $\frac{\partial f_1}{\partial E_{equ}}$, $\frac{\partial f_2}{\partial \theta_{equ}}$, as well as matrices $(I - (\frac{\partial f_1}{\partial E_{equ}})^{-1} \frac{\partial f_1}{\partial \theta_{equ}} (\frac{\partial f_2}{\partial \theta_{equ}})^{-1} \frac{\partial f_2}{\partial E_{equ}})$ and $(I - (\frac{\partial f_2}{\partial \theta_{equ}})^{-1} \frac{\partial f_2}{\partial E_{equ}} (\frac{\partial f_1}{\partial E_{equ}})^{-1} \frac{\partial f_1}{\partial \theta_{equ}})$ are full rank. From implicit function theorem in [17], within a small neighborhood where the Jacobian is full rank, $(P_{equ}, Q_{equ}, \theta_{equ}, E_{equ}, \omega_{equ})$ is isolated. ■

An equilibrium point $(P_{equ}, Q_{equ}, \theta_{equ}, E_{equ}, \omega_{equ})$ is achieved by designating commands $\{P_{ref,i}\}$ and $\{E_{ref,i}\}$ to droop controllers. This equilibrium point is usually determined as solutions to optimal power flow (OPF) problems. Based on equations (10,11,12), voltage and real power reference commands are then determined. Command $E_{ref,i}$ and $P_{ref,i}$ at bus $i$ are determined by

$$E_{ref,i} = E_{equ,i} + \frac{m_Q}{K_Q}(Q_{equ,i} + Q_{load,i}(E_{equ})), \tag{13}$$

$$P_{ref,i} = P_{equ,i} + P_{load,i}(E_{equ}) + D(\omega_{equ} - \omega_0). \tag{14}$$

About the existence of an isolated equilibrium point, the following assumption is made:

*Assumption 2:* Each equilibrium point $(P_{equ}, Q_{equ}, \theta_{equ}, E_{equ}, \omega_{equ})$ is assumed to be a solution to some OPF problem and to satisfy the conditions in Lemma 1, so that it is an isolated equilibrium point in a small neighborhood.

To derive a more general model for frequency synchronization analysis, phase angle dynamics in equation (7) are formulated as nonlinear oscillators. By inserting equations (1) and (3) into the swing equation, the equation (7) is then written as

$$\begin{aligned} M\ddot{\delta}_i + D\dot{\delta}_i &= P_{ref,i} - P_i - P_{load,i}, \\ &= P_{ref,i} - E_i^2 G_{ii} - P_{load,i}(E) - \sum_{j=1,j\neq i}^{n} E_i E_j (G_{ij}\cos(\delta_i - \delta_j) + B_{ij}\sin(\delta_i - \delta_j)), \\ &= \omega_{0,i} - \sum_{j=1,j\neq i}^{n} E_i E_j |Y_{ij}| \sin(\delta_i - \delta_j + \phi_{ij}), \end{aligned} \tag{15}$$

for all $i \in \{1, 2, \ldots, m+g\}$, where the natural frequency is $\omega_{0,i} = P_{ref,i} - P_{load,i}(E) - E_i^2 G_{ii}$; phase shift between bus $i$ and $j$, $\phi_{ij} = \phi_{ji} = \tan^{-1}(G_{ij}/B_{ij}) \in [-\frac{\pi}{2}, 0]$; the diagonal terms are $|Y_{ii}| = 0$ and $\phi_{ii} = 0$.

Power distribution networks coupled with both inverter-based DG's and pure loads are modeled as a hybrid network. An $n$-bus distribution network includes $m$ buses tied to inverter based DG's and $l$ pure load buses. Frequency synchronization model of this hybrid network is as follows

$$\begin{aligned} M\ddot{\delta}_i + D\dot{\delta}_i &= \omega_{0,i} - \sum_{j=1,j\neq i}^{n} E_i E_j |Y_{ij}| \sin(\delta_i - \delta_j + \phi_{ij}), \\ & \quad i \in \{1, \ldots, m+g\} \\ \dot{\delta}_i &= \frac{\sum_{j=1,j\neq i}^{n} E_i E_j |Y_{ij}| \cos(\delta_i - \delta_j + \phi_{ij})\dot{\delta}_j}{\sum_{j=1,j\neq i}^{n} E_i E_j |Y_{ij}| \cos(\delta_i - \delta_j + \phi_{ij})}, \\ & \quad i \in \{m+g+1, \ldots, m+g+l\} \end{aligned}$$

where $\omega_{0,i} = P_{ref,i} - P_{load,i}(E) - E_i^2 G_{ii}$ is the natural frequency of the nonlinear oscillator at bus $i$. Based on the hybrid network of nonlinear oscillators above, frequency synchronization is defined as asymptotic convergence of network frequency, as follows

*Definition 1:* The power distribution network has frequency synchronization if there are two open subsets of $\Omega_{E,1}, \Omega_{\theta,1} \subset \mathbb{R}^n$ containing the origin such that if any $\tilde{E}_i(0) \in \Omega_{E,1}$ and any $\theta_i(0) = (\delta_i(0) - \delta_n(0)) \in \Omega_{\theta,1}$ then $\lim_{t\to\infty} \dot{\delta}_1(t) = \ldots = \lim_{t\to\infty} \dot{\delta}_n(t) = \omega_{equ}$, when the inputs $P_{ref}$, $P_{load,a}$, $P_{load,b}$, $P_{load,c}$, $E_{ref}$, $Q_{load,a}$, $Q_{load,b}$, $Q_{load,c}$ are constant.

Voltage control dynamic model is based on the isolated equilibrium point that satisfies conditions in Lemma 1. Based on the isolated equilibrium point corresponding to a given set of commands, error states are define for phase angle, voltage magnitude and reactive power error vectors as $\tilde{\theta} = \theta - \theta_{equ}$, $\tilde{E} = E - E_{equ}$, and $\tilde{Q} = Q_{equ} - Q$. Voltage error dynamics model is:

$$\begin{aligned}
\dot{\tilde{E}}_i &= \dot{E}_i - \dot{E}_{equ,i}, \\
&= K_Q(E_{equ,i} - E_i) + m_Q(Q_{equ,i} - Q_i) + m_Q(Q_{load,i}(E_{equ,i}) - Q_{load,i}(E_i)), \\
&= m_Q\tilde{Q}_i - \left\{ K_Q + m_Q[Q_{load,b,i} + (2E_{equ,i} + \tilde{E}_i)Q_{load,a,i}] \right\} \tilde{E}_i, \\
&= m_Q \left\{ \tilde{Q}_i - Q_{load,a,i}\tilde{E}_i^{\,2} - [\frac{K_Q}{m_Q} + (Q_{load,b,i} + 2Q_{load,a,i}E_{equ,i})]\tilde{E}_i \right\}, \qquad (16) \\
&\quad i \in \{1, \ldots, m+g\}
\end{aligned}$$

$$\begin{aligned}
\tilde{Q}_i &= Q_{load,a,i}\tilde{E}_i^2 + (2Q_{load,a,i}E_{equ,i} + Q_{load,b,i})\tilde{E}_i. \qquad (17) \\
&\quad i \in \{m+g+1, \ldots, m+g+l\}
\end{aligned}$$

Equation (17) shows an algebraic relation between voltage magnitude and reactive power error vectors. With respect to the voltage error dynamics model above, it is possible to define voltage stability of the power distribution network, as follows

*Definition 2:* The power distribution network has voltage stability if there are two open subsets of $\Omega_{E,2}, \Omega_{\theta,2} \subset \mathbb{R}^n$ containing the origin such that if any $\tilde{E}_i(0) \in \Omega_{E,2}$ and any $\theta_i(0) = (\delta_i(0) - \delta_n(0)) \in \Omega_{\theta,2}$ then $\lim_{t\to\infty} \tilde{E}_1(t) = \ldots = \lim_{t\to\infty} \tilde{E}_n(t) = 0$, when the inputs $P_{ref}$, $P_{load,a}$, $P_{load,b}$, $P_{load,c}$, $Q_{ref}$, $Q_{load,a}$, $Q_{load,b}$, $Q_{load,c}$ are constant.

## IV. Main Result

This section derives sufficient conditions for voltage stability and frequency synchronization in a weak power distribution network coupled with both rotational and electronic DG's. These sufficient stability conditions are in the form of network weakness, control authority, and load levels. As long as these conditions are satisfied, the network asymptotically converges to the designated equilibrium point $(P_{equ}, Q_{equ}, \theta_{equ}, E_{equ}, \omega_{equ})$. Grid-connected case is then discussed, addressing concerns of how to manage DG's without affecting network stability. Voltage control analyses are the same as in our previous conference paper [18], however, proofs of voltage stability are included to make this paper self-sufficient. As in [18], the coupled voltage and

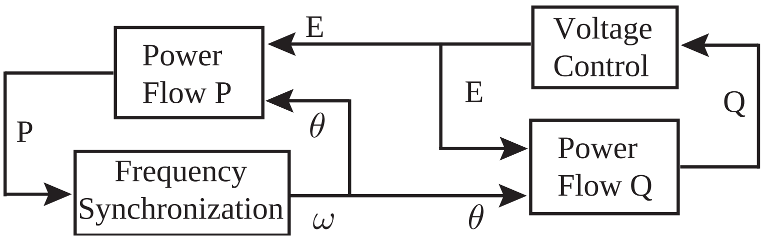


Fig. 2. Complete Model of the Network

frequency dynamics are solved by segmenting the entire system model into interconnected blocks, including a voltage control block, a frequency synchronization block, and two power balance blocks, as shown in Figure 2. Based on the segmented system model, stability analysis decouples by first identifying the existence of voltage magnitude and phase angle invariant sets; then proving asymptotic stability of both phase angle difference and voltage; finally establishing frequency synchronization.

### A. Invariant Sets

With no assumption on phase angles differences $\theta$, a positive invariant set of voltage magnitudes $\mathcal{I}_E$ is identified. Since relationships between voltage and reactive power errors on pure load buses are purely algebraic in equation (17), only dynamics on DG-coupled buses are considered. The following lemma characterizes a positive invariant set of voltage magnitudes $\mathcal{I}_E$.

*Lemma 2:* Consider the system model in equations (3,4,15,16), with $|\tilde{\theta}_i| \leq 2\pi$ for any $i \in$

$\{1, 2, \ldots, m+g\}$. Given

$$|Q_{load,a,i}| < a, \tag{18}$$

$$\begin{aligned} K_Q/m_Q > \max(&b_1 - Q_{load,b,i} + 2\sqrt{(a - Q_{load,a,i})c}, \\ &-b_2 - Q_{load,b,i} + 2\sqrt{(Q_{load,a,i} + a)c}), \end{aligned} \tag{19}$$

where

$$a = (2+4\pi)|G_{ii}|_{max} + (4+4\pi)|B_{ii}|_{max}, \tag{20}$$

$$b_1 = ((2+8\pi)|G_{ii}|_{max} + (4+8\pi)|B_{ii}|_{max} - 2Q_{load,a,i}) \max_i(E_{equ,i}), \tag{21}$$

$$b_2 = ((2+8\pi)|G_{ii}|_{max} + (4+8\pi)|B_{ii}|_{max} + 2Q_{load,a,i}) \max_i(E_{equ,i}), \tag{22}$$

$$c = 4\pi(|G_{ii}|_{max} + |B_{ii}|_{max})(\max_i(E_{equ,i}))^2. \tag{23}$$

If for each voltage magnitude $E_i$,

$$\tilde{E}_{-,l} \le E_i(0) - E_{equ,i} \le \tilde{E}_{+,u}, \tag{24}$$

then there exists a non-empty set

$$\mathcal{I}_E = \{E \in \mathbb{R}^m : E_{min} \le E_i \le E_{max}, 0 < E_{min} < E_{max}\},$$

where $E_{min} = \min_i(E_{equ,i}) + \min(0, \tilde{E}_{-,u})$ and $E_{max} = \max_i(E_{equ,i}) + \max(0, \tilde{E}_{+,l})$,

where there are,

$$\tilde{E}_{+,u}, \tilde{E}_{+,l} = \frac{K_Q/m_Q + Q_{load,b,i} - b_1}{2(a - Q_{load,a,i})} \pm \frac{\sqrt{(b_1 - K_Q/m_Q - Q_{load,b,i})^2 - 4(a - Q_{load,a,i})c}}{2(a - Q_{load,a,i})},$$

$$\tilde{E}_{-,u}, \tilde{E}_{-,l} = -\frac{K_Q/m_Q + Q_{load,b,i} + b_2}{2(Q_{load,a,i} + a)} \pm \frac{\sqrt{(b_2 + K_Q/m_Q + Q_{load,b,i})^2 - 4(Q_{load,a,i} + a)c}}{2(Q_{load,a,i} + a)},$$

The nonempty set $\mathcal{I}_E$ is positively invariant with respect to equations (3,4,15,16).

*Proof:* $\mathcal{I}_E$ will be an invariant set, if for arbitrary $i \in \{1, 2, \ldots m+g\}$, $|\tilde{E}_i|$ is non-increasing on the border of $\mathcal{I}_E$, with two cases to be considered. When there is $\tilde{E}_i = E_i - E_{equ,i} > 0$. Inserting equation (28) into equation (16) yields

$$\begin{aligned} \dot{\tilde{E}}_i &\le -[K_Q + m_Q(2E_{equ,i} + \tilde{E}_i)Q_{load,a,i} + Q_{load,b,i}]\tilde{E}_i + m_Q(l_E\tilde{E}_i + l_\delta 2\pi), \\ &= m_Q c + m_Q(-K_Q/m_Q - Q_{load,b,i} + b_1)\tilde{E}_i + m_Q(-Q_{load,a,i} + a)\tilde{E}_i^2. \end{aligned}$$

$\dot{\tilde{E}}_i$ should be non-positive to make $\tilde{E}_i$ non-increasing. Given the lemma's hypothesis (18,19), the equation $(-Q_{load,a,i} + a)x^2 + (-K_Q/m_Q - Q_{load,b,i} + b_1)x + c = 0$ has two real solutions, at least one of them being positive. If $\tilde{E}_{+,l} \leq \tilde{E}_i \leq \tilde{E}_{+,u}$ is satisfied, then $\tilde{E}_i$ is not increasing when $\tilde{E}_i > 0$.

The other case is $\tilde{E}_i < 0$. Similarly,

$$\begin{aligned}\dot{\tilde{E}}_i &\geq -[K_Q + m_Q(2E_{equ,i} + \tilde{E}_i)Q_{load,a,i} + Q_{load,b,i}]\tilde{E}_i - m_Q(l_E\tilde{E}_i + l_\delta 2\pi),\\ &= -m_Q c - m_Q(K_Q/m_Q + Q_{load,b,i} + b_2)\tilde{E}_i - m_Q(Q_{load,a,i} + a)\tilde{E}_i^2.\end{aligned}$$

$\dot{\tilde{E}}_i$ should be non-negative to make $\tilde{E}_i$ non-decreasing. Given the lemma's hypothesis (18,19), the equation $(Q_{load,a,i} + a)x^2 + (K_Q/m_Q + Q_{load,b,i} + b_2)x + c = 0$ has two real solutions, at least one of them being negative. If $\tilde{E}_{-,l} \leq \tilde{E}_i \leq \tilde{E}_{-,u}$ is satisfied, then $\tilde{E}_i$ is non-decreasing when $\tilde{E}_i < 0$.

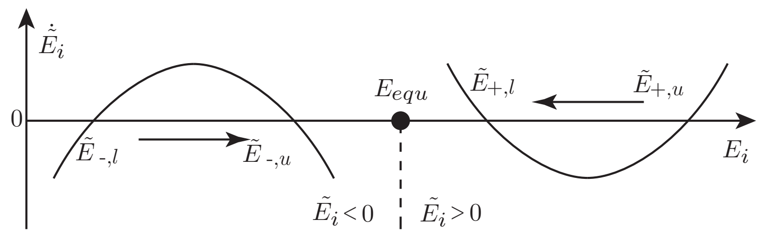


Fig. 3. Illustration of Voltage Invariant Set

Existence of an invariant set of voltage is demonstrated in Figure 3. The $x$-axis in the figure is the voltage magnitude $E_i$ at bus $i$, and the $y$-axis is the derivative of voltage error $\dot{\tilde{E}}_i$. Separated by $E_{equ,i}$, voltage error dynamics are discussed with both $\tilde{E}_i < 0$ and $\tilde{E}_i > 0$. If conditions in equations (18,19) are satisfied, two quadratic curves cross the $x$-axis where $\dot{\tilde{E}}_i = 0$. When $\tilde{E}_i > 0$, there is a convex quadratic curve, with cross points $\{\tilde{E}_{+,l}, \tilde{E}_{+,u}\}$. When $\tilde{E}_i < 0$, there is a concave quadratic curve, with cross points $\{\tilde{E}_{-,l}, \tilde{E}_{-,u}\}$. If an initial voltage error $\tilde{E}_i(0)$ lies between either $\{\tilde{E}_{+,l}, \tilde{E}_{+,u}\}$ or $\{\tilde{E}_{-,l}, \tilde{E}_{-,u}\}$, $E_i(t)$ approaches to cross points that are closer to $E_{equ}$, i.e. with $\tilde{E}_{+,l}$ and $\tilde{E}_{-,u}$ respectively. For any $i \in \{1, 2, \ldots, m+g\}$, $\tilde{E}_i$ stays in $\mathcal{I}_E$ once it starts between $\tilde{E}_{-,l}$ and $\tilde{E}_{+,u}$, so that equation (24) implies that $\mathcal{I}_E$ is positively invariant. ■

As voltages are bounded within $\mathcal{I}_E$, a condition is determined for a positive invariant set of phase angles, such that phase angle differences are kept bounded. The "Power Flow P" block and the "Frequency Synchronization" block, in Figure 2, are involved to prove bounded phase angle differences. Drawing upon techniques used in [10][13], the following lemma characterizes a positive invariant set of phase angle differences $\{\theta_i\}$.

*Lemma 3:* Assume the conditions in lemma 2 are satisfied. Define

$$A_1 = nE_{\min}^2 \min_{i\neq j}(|B_{ij}|),$$
$$A_2 = \max_{i\neq j}(|\omega_{0,i} - \omega_{0,j}|) - 2E_{min}^2 |G_{ii}|_{min},$$
$$\text{with} \quad \omega_{0,i} = P_{ref,i} - P_{load,i}(E) - E_i^2 G_{ii},$$

where $E_{\min}$ and $E_{\max}$ are from the set $\mathcal{I}_E$ in lemma 2. If

$$A_1 \sin(\theta) \geq A_2, \tag{25}$$

then there exists a non-empty set

$$\mathcal{I}_\theta = \{\theta \in \mathbb{R}^m : \max_{i,j}(|\theta_i - \theta_j|) \leq \theta, \theta \in [0, \pi]\},$$

which is positively invariant with respect to equations (3,4,15,16).

*Proof:* Define a positive function $V_\theta(\theta) : \mathbb{R}^{(m+g)} \to [0, \pi]$ for the $(m+g)$-bus network as

$$V_\theta(\theta) = \frac{1}{m_P} \max_{i\neq j}(|\theta_i - \theta_j|) = \frac{1}{m_P}(\theta_k - \theta_l),$$

where the $k$th bus achieves clockwise maximum $\theta_k$ and the $l$th bus achieves the counterclockwise minimum $\theta_l$, with $k, l \in \{1, 2, \ldots, m+g\}$. Assume that $|\theta_i(0) - \theta_j(0)| \leq \theta$ for any $i, j \in \{1, 2, \ldots, m+g\}$, where $\theta$ is arbitrary and $\theta \in [0, \pi]$, such that all angles are contained in an arc of length $\theta$. Since pure load buses have their phase angle dynamics determined by neighboring buses, the positive function $V_\theta$ only takes into account buses with DG's. Once states on DG-connected buses are determined, pure load buses' states are derived through algebraic relationships.

Taking the upper Dini derivative of $V_\theta$ to deal with discontinuity, there is

$$\begin{cases} D^+V_\theta = (\omega_k - \omega_l), \\ (\dot{\omega}_k - \dot{\omega}_l) = -\frac{D}{M}(\omega_k - \omega_l) + \frac{1}{M}u, \end{cases}$$

where there is input

$$\begin{aligned} u = {} & (\omega_{0,k} - \omega_{0,l}) \\ & -[\sum_{\substack{j=1 \\ j\neq k}}^{n} E_k E_j B_{kj} \sin(\theta_k - \theta_j) - \sum_{\substack{j=1 \\ j\neq l}}^{n} E_l E_j B_{lj} \sin(\theta_l - \theta_j)] \\ & -[\sum_{\substack{j=1 \\ j\neq k}}^{n} E_k E_j G_{kj} \cos(\theta_k - \theta_j) - \sum_{\substack{j=1 \\ j\neq l}}^{n} E_l E_j G_{lj} \cos(\theta_l - \theta_j)], \\ \leq {} & \max_{i\neq j}(|\omega_i - \omega_j|) - E_{\min}^2 n \min_{i\neq j}(|B_{ij}|) \sin\theta - 2E_{\min}^2 |G_{ii}|_{min}. \end{aligned}$$

Under the lemma's assumption in equation (25), there is $u \leq 0$, so that the value of $(\omega_k - \omega_l)$ always decreases to negative, whatever its initial $(\omega_k(0) - \omega_l(0))$ is. Since the upper Dini derivative $D^+V_\theta \leq 0$, then $V_\theta$ is non-increasing. As a result, $\mathcal{I}_\theta$ is a positively invariant set. ■

*Remark 1:* Equation (25) bounds network weakness in the form of $B_{ij}$ and $G_{ii}$, while the size of phase angle invariant set is larger for strong networks than weak ones. Similarity among controller natural frequencies $\{\omega_i\}$ improves frequency synchronization capability by increasing the size of phase shift ranges that are kept bounded.

These two positive invariant sets $\mathcal{I}_E$ and $\mathcal{I}_\theta$ provide bounded voltage magnitudes and phase angle differences to start with, asymptotic convergences of phase angle differences, voltages and the network frequency are then proved in the remainder of this section.

## B. Asymptotic Stability

Before proving asymptotic stability, in the sense of voltage control and frequency synchronization, the following lemma is established of maintaining a *Metzler* matrix with zero row sums when the system dynamics simplifies to a lower dimension. It is used when pure load buses are considered in frequency synchronization analysis.

*Lemma 4:* Assume that $F$ is a *Metzler* matrix with zero row sums, if matrix $F$ is written as a block matrix as $[F_1 \quad F_2; F_3 \quad F_4]$, in which $F_2$ and $F_3$ have non-zero elements on each row, then the matrix $(F_1 - F_2F_4^{-1}F_3)$ is also a *Metzler* matrix with zero row sums.

*Proof:* Since the matrix $F$ is a *Metzler* matrix with zero row sums, then there is $F_{ii} + \sum_{j=1,j\neq i}^{n} F_{ij} = 0$ and $|F_{ii}| = \sum_{j=1,j\neq i}^{n} F_{ij} = 0$. Based on *Gershgorin* theorem, matrix $F$ has all its eigenvalue disks centered at diagonal component values stay complete in the left-hand-side of the imaginary axis.

Because matrix $F_2$ has non-zero elements on each row, with $n = m + l$, diagonal block matrices $F_1$ have its row sums as follows

$$F_{1,ii} + \sum_{j=1,j\neq i}^{m} F_{1,ij} = -\sum_{j=1,j\neq i}^{l} F_{2,ij} < 0,$$

$$|F_{1,ii}| > \sum_{j=1,j\neq i}^{n} F_{1,ij} > 0.$$

Also based on *Gershgorin* theorem, matrix $F_1$ has all its eigenvalues with negative real parts. Similarly, matrix $F_4$ also has all its eigenvalues with negative real parts. Diagonal block matrices

$F_1$ and $F_4$ are both invertible.

Since matrix $(-F_4)$ is a nonsingular matrix with negative off-diagonal entries, whose eigenvalues all have positive real parts, then $(-F_4)$ is an *M-matrix* [19]. Based on characteristics of M-matrices, its inverse $(-F_4)^{-1}$ is nonnegative with all its elements nonnegative. Therefore, matrix $F_4$ is invertible, and all elements of the inverse matrix $F_4^{-1}$ are negative.

Expressing $F_4$ and $F_4^{-1}$ in row vectors $\{b_i\}$ and column vectors $\{a_i\}$, respectively, where $i \in \{1, \ldots, l\}$. Equation $F_4 F_4^{-1} = F_4^{-1} F_4 = I$ is rewritten as

$$F_4^{-1} F_4 = \begin{pmatrix} b_1 \\ b_2 \\ \vdots \\ b_l \end{pmatrix} \begin{pmatrix} a_1 & a_2 & \ldots & a_l \end{pmatrix} = \begin{pmatrix} b_1 a_1 & b_1 a_2 & \ldots & b_1 a_l \\ b_2 a_1 & b_2 a_2 & \ldots & b_2 a_l \\ \vdots & \vdots & \ddots & \vdots \\ b_l a_1 & b_l a_2 & \ldots & b_l a_l \end{pmatrix} = \begin{pmatrix} 1 & 0 & \ldots & 0 \\ 0 & 1 & \ldots & 0 \\ \vdots & \vdots & \ddots & \vdots \\ 0 & 0 & \ldots & 1 \end{pmatrix},$$

then $b_i \sum_{i=1}^{l} a_i = 1$ for each $i \in \{1, 2, \ldots, l\}$. Expressing $F_3$ in column vectors $\{c_j\}$, where $j \in \{1, \ldots, m\}$, then there is

$$F_4^{-1} F_3 = \begin{pmatrix} b_1 \\ b_2 \\ \vdots \\ b_l \end{pmatrix} \begin{pmatrix} c_1 & c_2 & \ldots & c_m \end{pmatrix} = \begin{pmatrix} b_1 c_1 & b_1 c_2 & \ldots & b_1 c_m \\ b_2 c_1 & b_2 c_2 & \ldots & b_2 c_m \\ \vdots & \vdots & \ddots & \vdots \\ b_l c_1 & b_l c_2 & \ldots & b_l c_m \end{pmatrix} = \begin{pmatrix} d_1 & d_2 & \ldots & d_m \end{pmatrix},$$

whose row sums are $b_i \sum_{i=1}^{m} c_i$ for all $i \in \{1, 2, \ldots, l\}$. Since each column vector $c_i$ are positive, $b_i c_j$ is negative for any $i$ and $j$. Since $F$ is a *Metzler* matrix with zero row sums, there is $\sum_{j=1}^{m} c_j + \sum_{j=1}^{l} a_j = 0$ for each $i \in \{1, 2, \ldots, l\}$, then each row sum has $b_i \sum_{j=1}^{m} c_j = -b_i \sum_{j=1}^{l} a_j = -1$. Since $b_i \sum_{j=1}^{m} c_j = -1$ and each $b_i c_j$ is negative, then there is $-1 \leq b_i c_j \leq 0$ and matrix $F_4^{-1} F_3$ has all its components negative. With matrix $F_2$ expressed as row vectors $\{e_j\}$, where $j \in \{1, \ldots, m\}$, then there is a square matrix

$$F_2 F_4^{-1} F_3 = \begin{pmatrix} e_1 d_1 & e_1 d_2 & \ldots & e_1 d_m \\ e_2 d_1 & e_2 d_2 & \ldots & e_2 d_m \\ \vdots & \vdots & \ddots & \vdots \\ e_m d_1 & e_m d_2 & \ldots & e_m d_m \end{pmatrix}.$$

Since each element of vector $d_j$ is between $-1$ and $0$, then there is $0 \leq -e_i d_i \leq \sum_{j=1}^{m} e_j$. Expressing matrix $F_1$ as row vectors $\{f_j\}$, then there is

$$F_1 - F_2 F_4^{-1} F_3 = \begin{pmatrix} f_1 \\ f_2 \\ \vdots \\ f_m \end{pmatrix} - \begin{pmatrix} e_1 d_1 & e_1 d_2 & \dots & e_1 d_m \\ e_2 d_1 & e_2 d_2 & \dots & e_2 d_m \\ \vdots & \vdots & \ddots & \vdots \\ e_m d_1 & e_m d_2 & \dots & e_m d_m \end{pmatrix},$$

in which each row is $f_i 1_m - e_i \sum_{i=1}^{m} d_i = 0$. Since there is $f_{ii} - e_i d_i \leq f_{ii} + \sum_{j=1}^{m} e_j \leq 0$, then each diagonal element $(f_{ii} - e_i d_i)$ is non-positive and all non-diagonal elements $f_{ij} - e_i d_j$ are positive. As a result, the matrix $F_1 - F_2 F_4^{-1} F_3$ is still a *Metzler* matrix with zero row sums. ■

Building upon the two invariant sets $\mathcal{I}_E$ and $\mathcal{I}_\theta$, asymptotic convergence of phase angle differences $\theta$ requires a stricter condition than the one in Lemma 3. Only two blocks are discussed, i.e. the "Power Flow P" block and the "Frequency Synchronization" block. The following theorem establishes sufficient conditions for phase angle differences convergence.

*Theorem 3:* Define $A_1 = nE_{\min}^2 \min_{i \neq j}(|B_{ij}|)$ and $A_2 = \max_{i \neq j}(|\omega_{0,i} - \omega_{0,j}|) - 2E_{min}^2 |G_{ii}|_{min}$, with $\omega_{0,i} = P_{ref,i} - P_{load,i}(E) - E_i^2 G_{ii}$. Under conditions in lemma 2 and 3, if

$$A_1 \sin(\pi/2 - \alpha_{\max}) \geq A_2, \tag{26}$$

where $\alpha_{\max} = \max_{i \neq j}(\tan^{-1}(\frac{-G_{ij}}{B_{ij}}))$, then there is $\lim_{t \to \infty} \theta_i(t) = \theta_{equ,i}$ for each $i \in \{1, 2, \dots, n\}$.

*Proof:* It is assumed that voltage magnitudes are constants and phase angles are states changing with time. Define $\alpha_{ij} = -\phi_{ij} = \tan^{-1}(-\frac{G_{ij}}{B_{ij}}) \in [0, \frac{\pi}{2}]$. Because natural frequency is $\omega_{0,i} = P_{ref,i} - P_{load,i}(E_i) - E_i^2 G_{ii}$ for bus $i$, it is not a function of phase angles $\delta_i$. Taking voltages as inputs, derivatives of equation (15) are

$$M \frac{d\ddot{\delta}_i}{dt} + D \frac{d\dot{\delta}_i}{dt} = -\sum_{\substack{j=1 \\ j \neq i}}^{n} E_i E_j |Y_{ij}| \cos(\delta_i - \delta_j - \alpha_{ij})(\dot{\delta}_i - \dot{\delta}_j) = F_i(t)\dot{\delta},$$

for $i \in \{1, 2, \dots, m+g\}$, where $F$ is a matrix whose components are

$$F_{ii}(t) = -\sum_{\substack{j=1 \\ j \neq i}}^{n} E_i E_j |Y_{ij}| \cos(\delta_i - \delta_j - \alpha_{ij}) \text{ and } F_{ij}(t) = E_i E_j |Y_{ij}| \cos(\delta_i - \delta_j - \alpha_{ij}).$$

Similarly for pure load buses, since $P_i + P_{load,i} = 0$ and $P_{load,i}$ is independent of frequency, then there is $0 = -\sum_{\substack{j=1 \\ j \neq i}}^{n} E_i E_j |Y_{ij}| \cos(\delta_i - \delta_j - \alpha_{ij})(\dot{\delta}_i - \dot{\delta}_j) = F_i(t)\dot{\delta}$ for $i \in \{m+g+1, m+g+2, \dots, m+g+l\}$ with $n = m+g+l$, where $F(t)$ has the same form as the DG-coupled buses.

By lemma 3 and setting $\theta = \pi/2 - \alpha_{max}$, for all $\theta_i, \theta_j \in \mathcal{I}_\theta$ where $i, j \in \{1, 2, \ldots, n\}$, there is $|\theta_i - \theta_j| = |\delta_i - \delta_j| < \frac{\pi}{2} - \alpha_{\max}$. This inequality simply means that $\cos(\delta_i - \delta_j - \alpha_{ij}) > 0$, then matrix $F(t)$ satisfies: (a) its off-diagonal elements are nonnegative and (b) its row sums are zero. As a result, $F(t)$ is a *Metzler* matrix with zero row sums for every time instant $t$.

With both dynamics of DGs and pure load buses, the complete system model is as follows, .

$$\frac{d}{dt}\begin{pmatrix} \dot{\delta}_{(m+g)\times 1} \\ \dot{\delta}_{l\times 1} \\ \dot{\omega}_{(m+g)\times 1} \\ \dot{\omega}_{l\times 1} \end{pmatrix} = \left(\begin{array}{cc|cc} 0 & 0 & I & 0 \\ 0 & 0 & 0 & I \\ \hline \frac{1}{M}F_1 & \frac{1}{M}F_2 & -\frac{D}{M}I & 0 \\ F_3 & F_4 & 0 & 0 \end{array}\right)\begin{pmatrix} \dot{\delta}_{(m+g)\times 1} \\ \dot{\delta}_{l\times 1} \\ \dot{\omega}_{(m+g)\times 1} \\ \dot{\omega}_{l\times 1} \end{pmatrix},$$

where, for any time instant $t$, block matrices $F_1$ and $F_4$ both have eigenvalues with pure negative real parts; $F_2$ and $F_3$ are non-zero matrices. It can be simplified to an $(m+g)$-dimensional system

$$M\frac{d}{dt}\ddot{\delta}_{(m+g)\times 1} + D\frac{d}{dt}\dot{\delta}_{(m+g)\times 1} = (F_1 - F_2F_4^{-1}F_3)\dot{\delta}_{(m+g)\times 1} = F_{sim}\dot{\delta}_{(m+g)\times 1}.$$

Based on lemma 4, the simplified matrix $F_{sim}$ preserves this property for any time instant $t$. Since the pure load buses decouple from other buses in the block matrix above, it is possible to remove states corresponding to pure load buses

$$\frac{d}{dt}\begin{pmatrix} \dot{\delta}_{(m+g)\times 1} \\ \dot{\omega}_{(m+g)\times 1} \end{pmatrix} = \left(\begin{array}{c|c} 0 & I \\ \hline \frac{1}{M}(F_1 - F_2F_4^{-1}F_3) & -\frac{D}{M}I \end{array}\right)\begin{pmatrix} \dot{\delta}_{(m+g)\times 1} \\ \dot{\omega}_{(m+g)\times 1} \end{pmatrix}.$$

Since $F_{sim}$ is still a *Metzler* matrix with zero row sums, then the proof of asymptotic frequency synchronization is identical for networks either with or without pure load buses. As long as frequencies at DG-coupled buses converge, pure load buses would take averaged frequencies to the same value as well.

For the simplicity of notation, the dynamics is written as $M\frac{d}{dt}\ddot{\delta}_{n\times 1} + D\frac{d}{dt}\dot{\delta}_{n\times 1} = F(t)\dot{\delta}_{n\times 1}$ with $n = m + g$. Taking the $n$th bus as a reference, then it is possible to rewrite the $2n$-dimensional system into a $2(n-1)$-dimensional one, whose lower-left block matrix $F_{(n-1)}(t)$ is as follows

$$\frac{d}{dt}\begin{pmatrix} \dot{\delta}_{(n-1)\times 1} \\ \dot{\omega}_{(n-1)\times 1} \end{pmatrix} = \left(\begin{array}{c|c} 0 & I \\ \hline \frac{1}{M}F_{(n-1)} & -\frac{D}{M}I \end{array}\right)\begin{pmatrix} \dot{\delta}_{(n-1)\times 1} \\ \dot{\omega}_{(n-1)\times 1} \end{pmatrix},$$

$$F_{(n-1)}(t) = \begin{pmatrix} F_{11} - F_{n1} & \cdots & F_{1(n-1)} - F_{n(n-1)} \\ \vdots & \ddots & \vdots \\ F_{(n-1)1} - F_{n1} & \cdots & F_{(n-1)(n-1)} - F_{n(n-1)} \end{pmatrix}.$$

Subtracting non-negative off-diagonal components of the $n$th row $F_{nj}$ for $j \in \{1, 2, \ldots, n-1\}$ shift components on the other $(n-1)$ rows to the negative direction. Based on Gershgorin theorem, matrix $F_{n-1}(t)$ has all its eigenvalues with negative real parts for every time instant $t$. The time-varying dynamic system above can be rewritten as

$$\frac{d}{dt}\begin{pmatrix} \dot{\theta}_{(n-1)\times 1} \\ \dot{\omega}_{(n-1)\times 1} - \dot{\omega}_n 1_{(n-1)\times 1} \end{pmatrix} = \frac{d}{dt}\begin{pmatrix} \dot{\theta}_{(n-1)\times 1} \\ \dot{\overline{\omega}}_{(n-1)\times 1} \end{pmatrix} = \left(\begin{array}{c|c} 0 & I \\ \hline \frac{1}{M}F_{(n-1)}(t) & -\frac{D}{M}I \end{array}\right)\begin{pmatrix} \dot{\theta}_{(n-1)\times 1} \\ \dot{\overline{\omega}}_{(n-1)\times 1} \end{pmatrix},$$

where $\overline{\omega}_i = \omega_i - \omega_n$ for any $i \in \{1, 2, \ldots, (n-1)\}$.

Define a candidate Lyapunov function, with positive definite weighting matrices, as

$$V_{[\dot{\theta},\dot{\overline{\omega}}]} = \begin{pmatrix} \dot{\theta}^T_{(n-1)\times 1} & \dot{\overline{\omega}}^T_{(n-1)\times 1} \end{pmatrix}\begin{pmatrix} k(\frac{D}{M})^2 I & k\frac{D}{M}I \\ k\frac{D}{M}I & I \end{pmatrix}\begin{pmatrix} \dot{\theta}_{(n-1)\times 1} \\ \dot{\overline{\omega}}_{(n-1)\times 1} \end{pmatrix}$$
$$+\frac{1}{M}\dot{\theta}^T_{(n-1)\times 1}(-F^T_{(n-1)} - F_{(n-1)})\dot{\theta}_{(n-1)\times 1},$$

where $0 \le k \le 1$. With symmetric matrix $(F^T_{(n-1)} + F_{(n-1)})$ being negative definite for any time instant $t$, the function above is bounded as $k_1\|[\dot{\theta},\dot{\overline{\omega}}]\|^2 \le V_{[\dot{\theta},\dot{\overline{\omega}}]} \le k_2\|[\dot{\theta},\dot{\overline{\omega}}]\|^2$, where $k_1$ and $k_2$ are both positive constants. Derivative of this candidate Lyapunov function is then $\dot{V}_{[\dot{\theta},\dot{\overline{\omega}}]} = \frac{1}{M}\dot{\theta}^T_{(n-1)\times 1}[-(\dot{F}^T_{(n-1)} + \dot{F}_{(n-1)}) + \frac{k}{\tau_S}(F^T_{(n-1)} + F_{(n-1)})]\dot{\theta}_{(n-1)\times 1} + \frac{k-1}{\tau_S}\dot{\overline{\omega}}^T_{(n-1)\times 1}\dot{\overline{\omega}}_{(n-1)\times 1}$.

Although symmetric matrix $(\dot{F}^T_{(n-1)} + \dot{F}_{(n-1)})$ is not definite, if the time constant $\tau_S$ is small enough, it is still able to bound $\dot{V}_{[\dot{\theta},\dot{\overline{\omega}}]}$ with $\dot{V}_{[\dot{\theta},\dot{\overline{\omega}}]} \le -k_3\|[\dot{\theta},\dot{\overline{\omega}}]\|^2$, where $k_3$ is a positive constant. According to theorem 4.10 in [20], the dynamical system is asymptotically stable with respect to its origin, so that frequency synchronizes to a single value, i.e. frequency synchronization. As a result, there is $\dot{\theta}_i$ asymptotically converging to zero, i.e. each $\theta_i(t) = \delta_i(t) - \delta_n(t)$ converges to a constant value.

Based on the hybrid network model of phase angles, by applying $(\dot{\delta}_i - \dot{\delta}_n)$ for each $i \in \{1, 2, \ldots, n-1\}$, there is

$$M(\dot{\omega}_i - \dot{\omega}_n) - D(\dot{\delta}_i - \dot{\delta}_n)$$
$$= (\omega_{0,i} - \omega_{0,n}) - (\sum_{j=1,j\neq i}^{n} E_iE_j|Y_{ij}|\sin(\delta_i - \delta_j + \phi_{ij}) - \sum_{j=1}^{n-1} E_nE_j|Y_{nj}|\sin(\delta_n - \delta_j + \phi_{nj})).$$

A linearized model for phase angle analysis can be derived with respect to the equilibrium point $\theta_{equ}$. There is an $2(n-1)$-dimensional model as follows

$$\begin{pmatrix} \dot{\tilde{\theta}}_{(n-1)\times 1} \\ \dot{\tilde{\omega}}_{(n-1)\times 1} - \dot{\tilde{\omega}}_n 1_{(n-1)\times 1} \end{pmatrix} = \begin{pmatrix} \dot{\tilde{\theta}}_{(n-1)\times 1} \\ \dot{\tilde{\overline{\omega}}}_{(n-1)\times 1} \end{pmatrix} = \left(\begin{array}{c|c} 0 & I \\ \hline F_{(n-1)}(t) & -\frac{D}{M}I \end{array}\right)\begin{pmatrix} \tilde{\theta}_{(n-1)\times 1} \\ \tilde{\overline{\omega}}_{(n-1)\times 1} \end{pmatrix},$$

where $\tilde{\tilde{\omega}}_i = \tilde{\omega}_i - \tilde{\omega}_n$ for any $i \in \{1, 2, \dots, (n-1)\}$.

Define another candidate Lyapunov function for this linearized system model as

$$V_{[\tilde{\theta},\tilde{\tilde{\omega}}]} = \begin{pmatrix} \tilde{\theta}^T_{(n-1)\times 1} & \tilde{\tilde{\omega}}^T_{(n-1)\times 1} \end{pmatrix} \begin{pmatrix} k^{'}(\frac{D}{M})^2 I & k^{'}\frac{D}{M} I \\ k^{'}\frac{D}{M} I & I \end{pmatrix} \begin{pmatrix} \tilde{\theta}_{(n-1)\times 1} \\ \tilde{\tilde{\omega}}_{(n-1)\times 1} \end{pmatrix}$$
$$+\frac{1}{M}\tilde{\theta}^T_{(n-1)\times 1}(-F^T_{(n-1)} - F_{(n-1)})\tilde{\theta}_{(n-1)\times 1},$$

where $0 \leq k^{'} \leq 1$. The function above is bounded as $k_1^{'}\|[\tilde{\theta},\tilde{\tilde{\omega}}]\|^2 \leq V_{[\tilde{\theta},\tilde{\tilde{\omega}}]} \leq k_2^{'}\|[\tilde{\theta},\tilde{\tilde{\omega}}]\|^2$, where $k_1^{'}$ and $k_2^{'}$ are both positive constants. Derivative of this candidate Lyapunov function is then $\dot{V}_{[\tilde{\theta},\tilde{\tilde{\omega}}]} = \frac{1}{M}\tilde{\theta}^T_{(n-1)\times 1}[-(\dot{F}^T_{(n-1)} + \dot{F}_{(n-1)}) + \frac{k^{'}}{\tau_S}(F^T_{(n-1)} + F_{(n-1)})]\tilde{\theta}_{(n-1)\times 1} + \frac{k^{'}-1}{\tau_S}\tilde{\tilde{\omega}}^T_{(n-1)\times 1}\tilde{\tilde{\omega}}_{(n-1)\times 1}$.

If the time constant $\tau_S$ is small enough, it is still able to bound $\dot{V}_{[\tilde{\theta},\tilde{\tilde{\omega}}]} \leq -k_3^{'}\|[\tilde{\theta},\tilde{\tilde{\omega}}]\|^2$, where $k_3^{'}$ is a positive constant. The original dynamical system is asymptotically stable with respect to its origin, so that there is asymptotic convergence of phase angle differences $\tilde{\theta}_{n-1}(t)$ to a zero vector. Since the linear model is with respect to $\theta_{equ}$, then phase angle differences $\theta_{n-1}(t)$ converge asymptotically to the equilibrium point to $\theta_{equ}$. Based on asymptotic stability theorem in [20], the original nonlinear system model is asymptotically stable with respect to $\theta_{equ}$. ∎

*Remark 2:* Equation (26) bounds the ratio $|G_{ij}/B_{ij}|$ of the weakest link within the network. Satisfying this condition ensures phase angle differences $\theta(t)$ converging to $\theta_{equ}$, once phase shifts reduce within the bound of $(\pi/2 - \alpha_{max})$.

As long as the phase angle differences asymptotically converge to an equilibrium point $\theta_{equ}$, voltage magnitudes of each bus are also asymptotically stabilized. The following theorem establishes the asymptotic voltage stability.

*Theorem 4:* Assume that conditions in lemma 2 and 3 as well as theorem 3 hold, then there is phase angle differences $\theta$ converging to $\theta_{equ}$ and voltage magnitudes within invariant set $\mathcal{I}_E$. Define $B_1$ and $B_2$ as

$$B_1 = \frac{K_Q}{m_Q} + \min_i(Q_{load,b,i} + (E_{equ,i} + E_i)Q_{load,a,i}),$$
$$B_2 = m_E.$$

If there is

$$B_1 > B_2, \tag{27}$$

then vector $\{E_i\}$ asymptotically converges to $\{E_{equ,i}\}$.

*Proof:* Because there is an algebraic relationship between $\tilde{Q}_i$ and $\tilde{E}_i$ for pure load buses, as shown in equation (17), it is only necessary to consider only buses with voltage droop control mechanisms. Define a positive function $V_E = \sum_{i=1}^{m+g} \frac{1}{2m_Q}\tilde{E}_i^2$. Taking the derivative of $V_E$

$$\begin{aligned}\dot{V}_E &= \sum_{i=1}^{m+g} \frac{1}{m_Q}\tilde{E}_i\dot{\tilde{E}}_i,\\ &= \tilde{Q}^T\tilde{E} - \tilde{E}^T\mathrm{diag}(\frac{\mathrm{K_Q}}{\mathrm{m_Q}} + \mathrm{Q_{load,b,i}} + (\mathrm{E_{equ,i}} + \mathrm{E_i})\mathrm{Q_{load,a,i}})\tilde{\mathrm{E}}.\end{aligned}$$

Because *Lemma* 3 and *Theorem* 3 imply convergence of vector $\{\theta_i\}$ to $\{\theta_{equ,i}\}$, for any $\epsilon_\theta$ there is a time $T$ such that when $t > T$ there is $|\tilde{\theta}_i|_{max} = |\theta_i - \theta_{equ,i}|_{max} < \epsilon_\theta$. Due to *Lemma* 6, $\|\tilde{Q}\|_2$ is bounded above by $m_E\|\tilde{E}\|_2 + \sqrt{m+g}m_\theta\epsilon_\theta$. As a result, the derivative of $V_E$ is bounded as,

$$\begin{aligned}\dot{V}_E \leq \sqrt{m+g}m_\theta\epsilon_\theta\sum_{i=1}^{m}|\tilde{E}_i|\\ + \tilde{E}^T\mathrm{diag}(\mathrm{m_E} - \frac{\mathrm{K_Q}}{\mathrm{m_Q}} - \mathrm{Q_{load,b,i}} - (\mathrm{E_{equ,i}} + \mathrm{E_i})\mathrm{Q_{load,a,i}})\tilde{\mathrm{E}}.\end{aligned}$$

For an arbitrary $\epsilon_\theta$, there is a subset of $\tilde{E}(t)$ satisfying

$$|\tilde{E}_i| < \frac{2\sqrt{m+g}m_\theta\epsilon_\theta}{-m_E + \frac{K_Q}{m_Q} + Q_{load,b,i} + (E_{equ,i} + E_i)Q_{load,a,i}},$$

for all $i \in \{1, 2, \ldots, m+g\}$. Under the theorem's assumption in equation (27), the denominator in the equation above is positive. Once $\tilde{E}(t)$ enters the subset at $t = T$, it stays in the set thereafter, i.e. the system is uniformly ultimately bounded. As $\epsilon_\theta$ goes to zero, $T$ increases and the size of the ultimate bound asymptotically goes to a zero vector. This is sufficient to imply asymptotic convergence of $\tilde{E}$ to zero, which further implies voltage stability. As a result, the voltage control block ensures the asymptotic convergence of voltage magnitudes $\{E_i\}$ to $\{E_{equ,i}\}$. ■

*Theorem 5:* Assume that conditions in lemma 2 and 3, as well as theorem 3 and 4 hold, then $\lim_{t\to\infty}\dot{\delta}_1(t) = \ldots = \lim_{t\to\infty}\dot{\delta}_n(t) = \omega_{equ}$ so that network frequency asymptotically converges to the equilibrium frequency $\omega_{equ}$.

*Proof:* Since conditions in lemma 2 and 3, as well as theorem 3 and 4 are all satisfied, then there is phase angle differences $\theta$ converging to $\theta_{equ}$ and voltage magnitudes $E$ converging to $E_{equ}$. Based on power balance relationships in equations (3,4), real and reactive power $P$ and $Q$ also converge to $P_{equ}$ and $Q_{equ}$, respectively. Since $P \to P_{equ}$ and $E \to E_{equ}$, phase angle dynamics in equation (5) is written as,

$$\lim_{t\to\infty}\dot{\delta}_i(t) = \frac{1}{D}(P_{ref,i} + D\omega_0 - P_{equ,i} - P_{load,i}(E_{equ,i})).$$

Bring expression of $P_{ref,i}$ in equation (14), for each DG-coupled bus $i$ there is $\lim_{t\to\infty}\dot{\delta}_i(t) = \frac{1}{D}(D\omega_{equ}) = \omega_{equ}$. Since frequencies on pure load buses are averages of their neighbors, the all $n$ buses have $\lim_{t\to\infty}\dot{\delta}_1(t) = \ldots = \lim_{t\to\infty}\dot{\delta}_n(t) = \omega_{equ}$, i.e. converging to the same $\omega_{equ}$. ■

### C. Extension to Grid-Connected Cases

To extend our analysis from islanded networks to general grid cases, a grid connection point must be included, which can be treated as an infinite bus. Different from a DG, this infinite bus maintains voltage and compensates for any real power imbalance. Such an infinite bus is approximated as a bus tied to a generator, whose control strengths of both phase angle and voltage are infinite. This fact makes stability conditions naturally satisfied, so that our stability analysis extends to grid-connected cases.

## V. Simulation Experiments

Our stability conditions not only ensure stability in weak power distribution networks coupled with both rotational and electronic DG's, but also provide guidance in how to connect these DG's to existing feeders. Simulation tests are conducted in two different models, one is a modified IEEE 37-bus distribution network and the other is a network based on a rural electrification project in Africa. The simulation result in the 37-bus test feeder shows how rotational DGs impact system stability under disturbances. These disturbances include load variations, as well as impulsive voltage changes, such as voltage sags caused by short-circuit faults and voltage surges due to machine start-ups. Simulating a network model used in the rural electrification project indicates how stability conditions are used in connecting multiple DG's to provide reliable power services to a larger area.

Simulation of the modified standard test feeder is done with both rotational and electronic DG's as shown in Figure 4, and it is compared to the case of a distribution network only tied to inverter-based DG's. Both networks are modified to be under power flow stress, so that they are *weak* networks. Four modifications are made to the standard test feeder in [21]: a) all load buses except bus $1$ are with $100$kW three-phase balanced constant impedance load; b) five additional DG's coupled at the ends of distribution feeders, whose total capacity is sufficient to supply all loads; c) DG's are connected through $1000$ feet "724" cables, as defined in [22]; d) the weak network operates at $480$V.

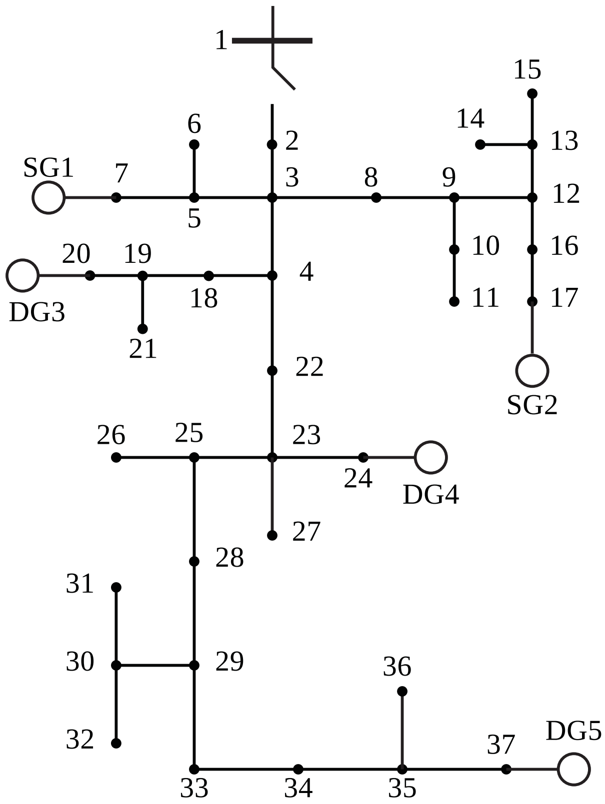


Fig. 4. Simulation 37-bus Test Feeder with 5 Distributed Generations

In the weak network, whose SCR is as small as four, the sufficient stability conditions ensures that the DG-coupled distribution network asymptotically converges to an equilibrium point. The equilibrium point is at $60$Hz, while the usual voltage regulatory limits of $\pm 5\%$ are relaxed. An OPF problem is formed to calculate the equilibrium point, whose voltage magnitudes stay between $0.69$p.u. and $1.44$p.u.. Conditions in *Lemma* 2 requires that $K_Q \geq 1600$, with $m_Q = 0.05$. The Jacobian in *Lemma* 1 is full rank, and conditions in *Lemma* 3, *Theorem* 3, and *Theorem* 4 are all satisfied. Both load level and voltage magnitude disturbances are applied to the weak network, which is coupled with both rotational and electronic DG's.

The following simulation test starts from connecting to the main grid; at $t = 50s$, the test feeder is islanded from the main grid by opening the primary switch between bus $1$ and $2$; at $t = 75s$, the load on all pure load buses increase by $40\%$ for five seconds. Both network frequency and voltage magnitudes converge to the equilibrium point, as shown in figure 5.

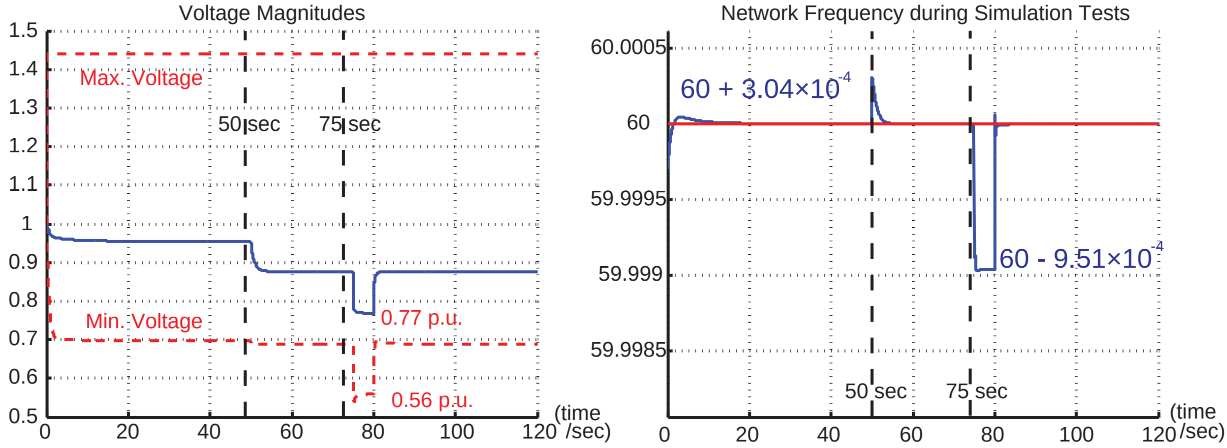


Fig. 5. Simulation Result of Weak Network Response to Changing Loads

In the left plot in figure 5, the upper and lower dash lines are the maximum and minimum voltages among all buses. The solid line represents the voltage magnitude at bus $2$. In the right plot, the network frequency is demonstrated in solid blue line, with a $60$Hz nominal value. During the islanding operation at $t = 50s$, the voltage envelop does not change. Within five seconds after islanding, both voltage magnitudes and network frequency converge to the equilibrium point. After the load increase at $t = 75s$, the maximum voltage decrease is less than $0.14$p.u., and the network frequency droops by as much as $9.51 \times 10^{-4}$Hz. In less than five seconds after all loads return to nominal values, network states restore to the equilibrium point. Under the same load level increase situation, the network coupled with only inverter-based DG's behaves similarly as shown in figure 5.

The following simulations show network response to voltage magnitude changes on buses tied to DG's, demonstrated in figure 6. After islanding from the main grid at $t = 50s$, network states converge to the equilibrium point in five seconds. At $t = 75s$, the voltage magnitude at SG $1$ is decreased by $0.9$p.u. and increased by $1.1$p.u.. The network response is shown as in figure 6

In the left plot of figure 6, the minimum voltage envelop drops to $0.52$p.u., in response to a $0.9$p.u. voltage sag at SG $1$. Voltage magnitudes restore to the equilibrium point in less than two seconds, so does the network frequency. In the right plot, the maximum voltage increases to $2.52$p.u., after the $1.1$p.u. voltage surge at SG $1$. Restoration of voltage and frequency takes less than two seconds. Going through the same voltage magnitude disturbances happened to SG $1$, the

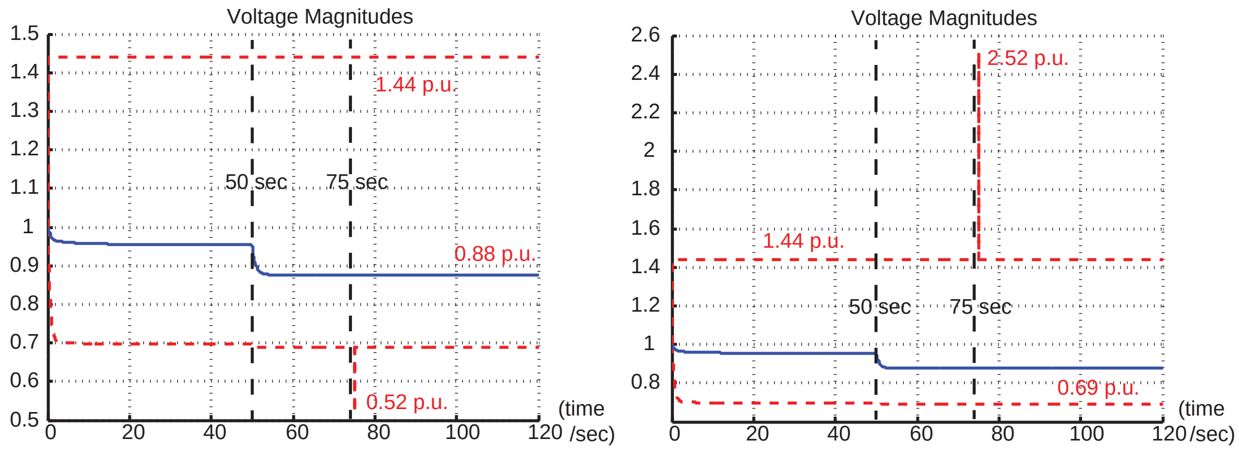


Fig. 6. Simulation Result of Weak Network Response to Voltage Changes at DGs

weak network tied only to inverter-based DG's also converge asymptotically to the equilibrium point. Their transients, however, are different due to dissimilar dynamics of DG's. In the figure 7,

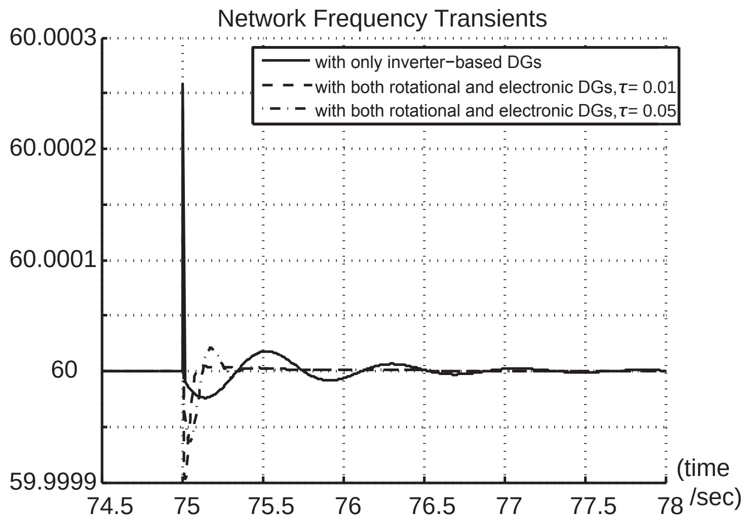


Fig. 7. Frequency Transients Comparison with Different DGs

the two weak networks behave differently during transients after the voltage surge at $t = 75s$. The network coupled with only inverter-based DG's oscillates and converges to $60$Hz within five seconds, represented in a solid line. The frequency transients, shown in dashed lines, converge much faster than the prior case. With a time constant $\tau = 0.01$, the network frequency restores in $0.2$ second with no oscillation. With a larger time constant $\tau = 0.05$, the response is slower, but still reaching the equilibrium point frequency within $0.5$ second. Consequently, with the second-order dynamics in swing equations of rotational DG's, the frequency oscillation caused by voltage magnitude disturbances is damped. As the time constant of power measurement units $\tau$ decreases, this damping effect becomes stronger. This additional low-pass filter, however, may have adverse impact on how the weak network can sustain load variations.

The African rural electrification project intends to provide reliable electric power to refugee camps where a national power grid is unavailable. Currently, distributed microgrids consist of diesel generators and solar panels are connected to provide electricity to schools, as shown in figure 8. The single-phase microgrids operate at $230$V and $50$Hz. Generation units include a $6.5$kW diesel generator, a $28.8$kWh battery bank, and $1250$W solar panels. There are three load buses, including an office (550W), an entrepreneurship center (570W), and dorms (240W). Links connecting all components within a microgrid are "$724$" cables, as defined in [22].

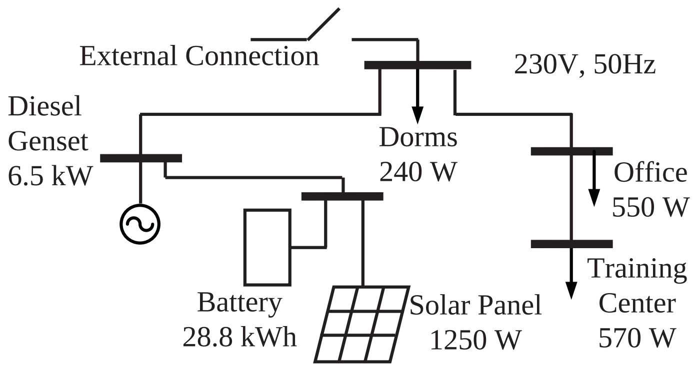


Fig. 8. Illustration of a Power Service Region

The next step is to expand power service areas by connecting several such microgrids together. The fundamental problem is wether such interconnections have an adverse impact on network stability. Sufficient stability conditions apply to this single-phase network and provide rule of thumbs in connecting multiple microgrids robustly. Assuming three similar microgrids are connected to a single node, which can be tied to a national grid in the future. Links between this node and all three regions are one-mile cables. The corresponding simulation network model is shown in Figure 9.

Local generation units are able to supply local loads within the microgrid in figure 8. Moreover,

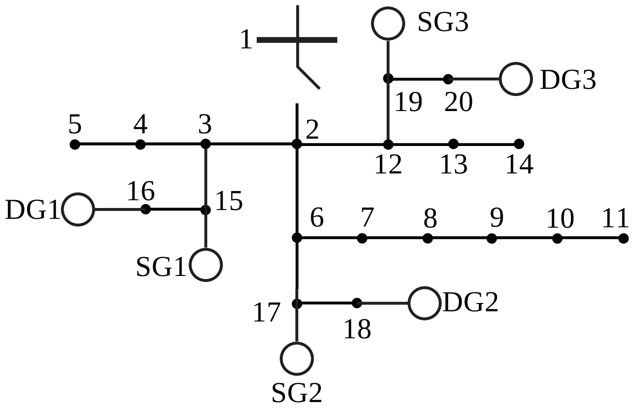


Fig. 9. Simulation Model of Rural Electrification Regions

to consider future expansions, the load level on each bus is doubled. Simulation tests are conducted to check responses to voltage magnitude disturbances at SG $1$. Two types of cables, “722” and “724” in [22], are chosen to link bus $2$ with bus $3$, bus $6$, and bus $12$, i.e. a load bus in each region, respectively. Using “722” cables, an equilibrium point is solved from an OPF problem, which commands all loads to be supplied by the local generator. The equilibrium point has a frequency of $50$Hz, and voltage magnitudes between $0.977$p.u. and $1.026$p.u.. Conditions in *Lemma* $3$, *Theorem* $3$, and *Theorem* $4$ are all satisfied. Response of voltage magnitudes and frequencies to a $1.1$p.u. voltage surge at SG $1$ is shown in Figure 10.

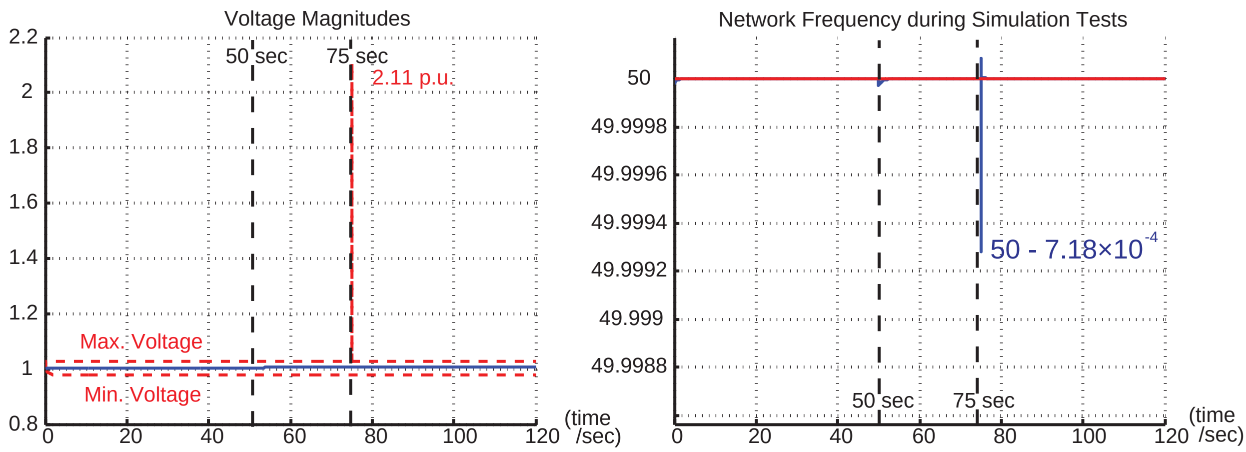


Fig. 10. Response of Rural Electrification Network to Voltage Changes at SG 1

In the left plot of figure 10, the upper and lower dash lines are the maximum and minimum voltages among all buses. The solid line represents the voltage magnitude at bus $2$. In the right plot, network frequency is demonstrated in a solid line, with a $50$Hz nominal value. During the islanding operation at $t = 50s$, the voltage envelop does not change. Within five seconds after islanding, both voltage magnitudes and network frequency converge to the equilibrium point. After the voltage increase at $t = 75s$, the maximum voltage increases to about $2.11$p.u., and the network frequency droops by as much as $7.18 \times 10^{-4}$Hz. In less than five seconds after the disturbance, network states restore to the equilibrium point. This simulation shows that the sufficient stability conditions are applicable to single-phase network models.

In contrast to the previous case, using “724” cables, it is not able to obtain an equilibrium point that satisfies stability conditions, especially conditions in *Lemma* 3 and *Theorem* 3. This is mainly due to the lossy property of cables that are used to connect these geographically distributed microgrids. Although there is little power flow through each cable during normal operations, coupled voltage and frequency dynamics drive the weak network to instability after voltage disturbances.

Lessons learned from simulations above include: i) although the second-order dynamics in swing equations help to smooth weak networks’ responses to voltage disturbances of DG’s, the delay may have an adverse impact on the networks’ ability to sustain load variations; ii) in the rural electrification project, simply connecting multiple microgrids using lossy cables will not guarantee robust power service to a larger area; iii) thick cables should be used to connect distributed regions to ensure stability, even though the generation capacity of each microgrid is much less than the power rating of such cables.

## VI. Summary

Asymptotic stability conditions are derived for *weak* power distribution networks, to which both rotational and electronic DG’s are coupled. These conditions take the form of inequality constraints on various network parameters, loads and generation control commands. Together with optimal power flow problems, network states are ensured to asymptotically converge to an equilibrium point. Simulation of a modified IEEE 37-node test feeder shows that these weak networks can sustain load variations and voltage magnitude disturbances of DG’s. Furthermore, these sufficient stability conditions guide the connection of multiple microgrids to provide reliable power services to a large area in a rural electrification project in Africa.

## APPENDIX

In the Appendix, *Lemma* 5 and *Lemma* 6 establish bounds on norms of $\tilde{Q}$ as functions of voltage and phase angle error vectors, i.e. $\tilde{E}$ and $\tilde{\theta}$.

*Lemma 5:* Defined $l_E$ and $l_\theta$ as

$$l_E = 2(\max_i(E_{equ,i}) + |\tilde{E}_i|_{max})(|G_{ii}|_{max} + 2|B_{ii}|_{max}),$$
$$l_\theta = 2(\max_i(E_{equ,i}) + |\tilde{E}_i|_{max})^2(|G_{ii}|_{max} + |B_{ii}|_{max}),$$

then absolute value of the reactive power error $|\tilde{Q}_i|$ is bounded by

$$|\tilde{Q}_i| \leq l_E|\tilde{E}_i|_{max} + l_\theta \cdot 2\pi. \tag{28}$$

*Proof:* With the help of its Jacobian $\partial Q/\partial E$ and $\partial Q/\partial\theta$, $\tilde{Q}$ is linearized as $\tilde{Q} = Q - Q_{equ} = \frac{\partial Q}{\partial E}\Big|_{equ}(E - E_{equ}) + \frac{\partial Q}{\partial \theta}\Big|_{equ}(\theta - \theta_{equ}) = \frac{\partial Q}{\partial E}\Big|_{equ}\tilde{E} + \frac{\partial Q}{\partial \theta}\Big|_{equ}\tilde{\theta}$. Taking infinite vector norms on both sides, there is

$$\begin{aligned}
\|\tilde{Q}\|_\infty &\leq \left\|\frac{\partial Q}{\partial E}\tilde{E} + \frac{\partial Q}{\partial \theta}\tilde{\theta}\right\|_\infty \leq \left\|\frac{\partial Q}{\partial E}\tilde{E}\right\|_\infty + \left\|\frac{\partial Q}{\partial \theta}\tilde{\theta}\right\|_\infty, \\
&\leq \left\|\frac{\partial Q}{\partial E}\right\|_\infty \left\|\tilde{E}\right\|_\infty + \left\|\frac{\partial Q}{\partial \theta}\right\|_\infty \left\|\tilde{\theta}\right\|_\infty, \\
\max_i(|\tilde{Q}_i|) &\leq \left\|\frac{\partial Q}{\partial E}\right\|_\infty \max_i(|\tilde{E}_i|) + \left\|\frac{\partial Q}{\partial \theta}\right\|_\infty \max_i(|\tilde{\theta}_i|),
\end{aligned}$$

where $\|\frac{\partial Q}{\partial E}\|_\infty$ and $\|\frac{\partial Q}{\partial \theta}\|_\infty$ are bounded as following

$$\begin{aligned}
\|\frac{\partial Q}{\partial E}\|_\infty &= \sum_{\substack{j=1 \\ j\neq i}} |E_i(G_{ij}\sin(\theta_i - \theta_j) - B_{ij}\cos(\theta_i - \theta_j))| \\
&\quad + |\sum_{\substack{j=1 \\ j\neq i}} E_i(G_{ij}\sin(\theta_i - \theta_j) - B_{ij}\cos(\theta_i - \theta_j)) - 2E_iB_{ii}|, \\
&\leq |2E_iB_{ii}| + 2\sum_{\substack{j=1 \\ j\neq i}} |E_i(G_{ij}\sin(\theta_i - \theta_j) - B_{ij}\cos(\theta_i - \theta_j))|, \\
&\leq 2\max_i(|E_i|)|B_{ii}|_{max} + 2\max_i(|E_i|)\max_i(\sum_{\substack{j=1 \\ j\neq i}}(|G_{ij}| + |B_{ij}|)), \\
&\leq 2(\max_i(E_{equ,i}) + \max_i(|\tilde{E}_i|))(|G_{ii}|_{max} + 2|B_{ii}|_{max}) = l_E,
\end{aligned}$$

$$
\begin{aligned}
\|\frac{\partial Q}{\partial \theta}\|_\infty = &|\sum_{\substack{j=1\\ j\neq i}} E_iE_j(G_{ij}\cos(\theta_i-\theta_j)+B_{ij}\sin(\theta_i-\theta_j))| \\
&+\sum_{\substack{j=1\\ j\neq i}} |E_iE_j(G_{ij}\cos(\theta_i-\theta_j)+B_{ij}\sin(\theta_i-\theta_j))|, \\
&\leq 2\sum_{\substack{j=1\\ j\neq i}} |E_iE_j(G_{ij}\cos(\theta_i-\theta_j)+B_{ij}\sin(\theta_i-\theta_j))|, \\
&\leq 2(\max_i(|E_i|))^2 \max_i(\sum_{\substack{j=1\\ j\neq i}}(|G_{ij}|+|B_{ij}|)), \\
&\leq 2(\max_i(E_{equ,i})+\max_i(|\tilde{E}_i|))^2(|G_{ii}|_{max}+|B_{ii}|_{max}) = l_\theta.
\end{aligned}
$$

■

*Remark 3:* Absolute value of reactive power error $|\tilde{Q}_i|$ is bounded as a function of equilibrium voltage magnitude $E_{equ,i}$, network link parameters $G_{ii}$ and $B_{ii}$, as well as maximum voltage error $|\tilde{E}_i|$. These expressions of $l_E$ and $l_\theta$ bound the derivative of voltage magnitude error $\dot{\tilde{E}}_i$ with a second order polynomial inequality.

*Lemma 6:* Define $m_E$ and $m_\theta$ as

$$
\begin{aligned}
m_E &= \max\{\sqrt{\lambda} : \lambda \text{ is an eigenvalue of } (\partial Q/\partial E)^*(\partial Q/\partial E)\}, \\
m_\theta &= \max\{\sqrt{\lambda} : \lambda \text{ is an eigenvalue of } (\partial Q/\partial \theta)^*(\partial Q/\partial \theta)\},
\end{aligned}
$$

then two-norm of the reactive power error vector $\tilde{Q}$ is bounded by

$$
\|\tilde{Q}\|_2 \leq m_E\|\tilde{E}\|_2 + \sqrt{n}m_\theta|\tilde{\theta}_i|_{\max}. \tag{29}
$$

*Proof:* If system frequency synchronizes to $\omega_{equ}$ and phase shifts are within the invariant set $\mathcal{I}_\theta$, then for any $i \in \{1,2,\dots,n\}$ there is a bounded $|\tilde{\theta}_i|$. Within the invariant set $\mathcal{I}_E$, applying vector two-norm and its induced matrix two-norm, there is

$$
\begin{aligned}
\|\tilde{Q}\|_2 &= \|\frac{\partial Q}{\partial E}\tilde{E} + \frac{\partial Q}{\partial \theta}\tilde{\theta}\|_2, \\
&\leq \|\frac{\partial Q}{\partial E}\tilde{E}\|_2 + \|\frac{\partial Q}{\partial \theta}\tilde{\theta}\|_2, \\
&\leq \|\frac{\partial Q}{\partial E}\|_2\|\tilde{E}\|_2 + \|\frac{\partial Q}{\partial \theta}\|_2\sqrt{n}\max_i(|\tilde{\theta}_i|), \\
&\leq m_E\|\tilde{E}\|_2 + \sqrt{n}m_\theta\max_i(|\tilde{\theta}_i|).
\end{aligned}
$$

■

*Remark 4:* Magnitude of reactive power error vector $\|\tilde{Q}\|_2$ is bounded as a weighted combination of voltage magnitude error vector magnitude $\|\tilde{E}\|_2$ and the maximum phase angle error $|\tilde{\theta}_i|$. The expressions of $m_E$ and $m_\theta$ are used to prove asymptotic voltage stability in section IV, by providing an ultimate uniform bound for voltage magnitude errors $\{\tilde{E}_i\}$.

## REFERENCE


[1] R. Lasseter, "Smart distribution: Coupled microgrids," *Proceedings of the IEEE*, vol. 99, no. 6, pp. 1074–1082, 2011.

[2] N. P. Strachan and D. Jovcic, "Stability of a variable-speed permanent magnet wind generator with weak ac grids," *Power Delivery, IEEE Transactions on*, vol. 25, no. 4, pp. 2779–2788, 2010.

[3] G. Gless, "Direct method of liapunov applied to transient power system stability," *Power Apparatus and Systems, IEEE Transactions on*, no. 2, pp. 159–168, 1966.

[4] A. El-Abiad and K. Nagappan, "Transient stability regions of multimachine power systems," *Power Apparatus and Systems, IEEE Transactions on*, no. 2, pp. 169–179, 1966.

[5] J. Willems and J. Willems, "The application of lyapunov methods to the computation of transient stability regions for multimachine power systems," *Power Apparatus and Systems, IEEE Transactions on*, no. 5, pp. 795–801, 1970.

[6] T. Athay, R. Podmore, and S. Virmani, "A practical method for the direct analysis of transient stability," *Power Apparatus and Systems, IEEE Transactions on*, no. 2, pp. 573–584, 1979.

[7] N. Martins, "Efficient eigenvalue and frequency response methods applied to power system small-signal stability studies," *Power Systems, IEEE Transactions on*, vol. 1, no. 1, pp. 217–224, 1986.

[8] L. Wang and A. Semlyen, "Application of sparse eigenvalue techniques to the small signal stability analysis of large power systems," in *Power Industry Computer Application Conference, 1989. PICA'89, Conference Papers*. IEEE, 1989, pp. 358–365.

[9] P. Kundur, G. Rogers, D. Wong, L. Wang, and M. Lauby, "A comprehensive computer program package for small signal stability analysis of power systems," *Power Systems, IEEE Transactions on*, vol. 5, no. 4, pp. 1076–1083, 1990.

[10] F. Dorfler and F. Bullo, "Synchronization and transient stability in power networks and non-uniform Kuramoto oscillators," vol. 50, no. 3, pp. 1616–1642, 2012.

[11] J. W. Simpson-Porco, F. Dorfler, and F. Bullo, "Synchronization and power sharing for droop-controlled inverters in islanded microgrids," *Automatica*, vol. 49, no. 9, pp. 2603 – 2611, 2013. [Online]. Available: http://www.sciencedirect.com/science/article/pii/S0005109813002884

[12] J. Schiffer, A. Anta, T. D. Trung, J. Raisch, and T. Sezi, "On power sharing and stability in autonomous inverter-based microgrids," in *Decision and Control (CDC), 2012 IEEE 51st Annual Conference on*. IEEE, 2012, pp. 1105–1110.

[13] F. Dörfler and F. Bullo, "On the critical coupling for kuramoto oscillators," *SIAM Journal on Applied Dynamical Systems*, vol. 10, no. 3, pp. 1070–1099, 2011.

[14] J. Schiffer, D. Goldin, J. Raisch, and T. Sezi, "Synchronization of droop-controlled microgrids with distributed rotational and electronic generation," *52nd IEEE CDC, Florence, Italy*, 2013.

[15] A. R. Bergen, *Power Systems Analysis, 2/E*. Pearson Education India, 2009.

[16] "Load representation for dynamic performance analysis [of power systems]," *Power Systems, IEEE Transactions on*, vol. 8, no. 2, pp. 472–482, 1993.

[17] K. Fritzsche and H. Grauert, *From holomorphic functions to complex manifolds*. Springer, 2002, vol. 213.

[18] Z. Wang, M. Xia, and M. Lemmon, “Voltage stability of weak power distribution networks with inverter connected sources,” in *American Control Conference, Washington DC, USA*, 2013.

[19] R. Plemmons, “M-matrix characterizations. iłnonsingular m-matrices,” *Linear Algebra and its Applications*, vol. 18, no. 2, pp. 175–188, 1977.

[20] H. K. Khalil, *Nonlinear systems*. Prentice hall Upper Saddle River, 2002, vol. 3.

[21] W. H. Kersting, “Radial distribution test feeders,” in *Power Engineering Society Winter Meeting, 2001. IEEE*, vol. 2. IEEE, 2001, pp. 908–912.

[22] D. S. A. Subcommittee, “Ieee 37 node test feeder,” IEEE, Tech. Rep., 2001.